Santa Clara University
Scholar Commons

Physics | College of Arts & Sciences

4-2-2017

Room-temperature self-powered energy photodetector based on optically induced Seebeck effect in Cd_3As_2

Niloufar Yavarishad

Tahereh Hosseini

Elaheh Kheirandish

Christopher P. Weber
Santa Clara University, cweber@scu.edu

Nikolai Kouklin

Follow this and additional works at: https://scholarcommons.scu.edu/physics

Part of the Condensed Matter Physics Commons

Recommended Citation
Yavarishad, N., Hosseini, T., Kheirandish, E., Weber, C. P., & Kouklin, N. (2017). Room-temperature self-powered energy photodetector based on optically induced Seebeck effect in Cd_3As_2. Applied Physics Express, 10(5), 052201. https://doi.org/10.7567/APEX.10.052201

This is an author-created, un-copyedited version of an article accepted for publication in insert |name of journal|. The publisher is not responsible for any errors or omissions in this version of the manuscript or any version derived from it. The Version of Record is available online at https://doi.org/10.7567/APEX.10.052201.

This Article is brought to you for free and open access by the College of Arts & Sciences at Scholar Commons. It has been accepted for inclusion in Physics by an authorized administrator of Scholar Commons. For more information, please contact rscroggin@scu.edu.

Room-temperature, self-powered energy photo-detector based on the optically-induced Seebeck effect in Cd_3As_2

Niloufar Yavarishad[1], Tahereh Hosseini[1], Elaheh Kheirandish[1], Chris P.Weber[2] and Nikolai Kouklin[1]

[1]Dept. of Electrical Engineering, Univ. of Wisconsin-Milwaukee, P.O. Box 413 Milwaukee, WI, 53201, USA

[2]Dept. of Physics, Santa-Clara University,500 El Camino Real Santa Clara, CA, 95053, USA

We demonstrate an intrinsically fast, Seebeck-type metal-semimetal-metal infrared photodetector based on Cd_3As_2 crystals. The Seebeck voltage is induced under off-center illumination, leading to asymmetric temperature gradients and net current flow. The sensor's room-temperature responsivity is 0.27 mA/W. The photocurrent signal is readily registered at a modulation frequency of 6 kHz, and the sensor's intrinsic bandwidth is predicted to approach terahertz. We find that the photocurrent depends on the optical power and modulation frequency. Our study reveals crystalline Cd_3As_2 as a promising material for high-bandwidth and spectrally broad photo-sensing, imaging, and communication.

Corresponding author email: nkouklin@uwm.edu

The development of modern opto-electronic systems is driven in part by steady improvements in the responsivity and spectral bandwidth of solid-state light sensors and image detectors. However, many low-cost solid-state detection systems still suffer from low internal gain, limited bandwidth, or large readout noise, making them ill-suited for application in optical communication, medical imaging, or scientific research. Moreover, the continuing reduction in the size of opto-electronic components necessitates the development of new classes of photo-sensing materials with a high gain-bandwidth product, improved stability against environmental effects and high responsivity in an ultra-wide spectral range that extends to the far infrared or terahertz. Energy photodetectors, such as bolometers, have spectral sensitivity extending beyond terahertz, but most energy detectors are inherently slow and exhibit extremely poor sensitivity.

Recent theoretical and experimental advances have led to the discovery of new classes of quantum materials, the topological insulators and Weyl and Dirac semimetals [1-3], which are highly promising for electronic applications. In three-dimensional Dirac semimetals, such as Na_3Bi and Cd_3As_2, electrons disperse linearly in momentum-space, as they do in two dimensions in graphene. Crystal symmetry protects the zero-energy node against gap formation, so interband absorption—and intrinsic spectral sensitivity—extends to terahertz frequencies in undoped material. Bulk Cd_3As_2 is more stable than other Dirac semimetals; compared to graphene, its electronic properties are well protected against changes to the surface or environment;its free-carrier mobility, up to 10^7 $cm^2V^{-1}s^{-1}$ at 5 K [4], approaches that of a two-dimensional electron gas in a GaAs/AlGaAs heterojunction [5]. Given its strong light absorption in the infrared, low thermal conductivity and large thermopower (about 600 μV/K in the temperature range of 300-400 K [6]), Cd_3As_2 holds promise for the development of spectrally-broad, high-

bandwidth photodetectors, optical switches and energy-converting photo-cells [7] based on the photo-induced Seebeck effect, also known as photo-thermo-voltaic (PTV) effect. In the Cd_3As_2 PTV sensors we demonstrate below, off-center illumination leads to asymmetric temperature gradients, which in turn cause a net flow of electrical current, even in the absence of an external bias.

We synthesized Cd_3As_2 planar crystals up to 1 cm long in a horizontally-oriented hot-wall Chemical Vapor Deposition (CVD) atmospheric pressure reactor. A ~99% pure polycrystalline Cd_3As_2 powder from Sigma-Aldrich was used as a precursor. To reduce the partial pressure of oxygen, the reactor was flushed several times by first lowering the base pressure to ~ 1 mTorr and then refilling with 99.99% pure Argon gas. The precursor vapors of Cd and As were transported with the help of the Argon gas at a rate of 0.1-0.2 SCCM. The reactor temperature was monitored with a thermocouple and gradually raised from room temperature to 700 °C. The synthesis proceeded for 2 hours, after which the reactor was allowed to cool down naturally at a typical rate of 5 °C min^{-1}. Large, shiny crystallites of Cd_3As_2 nucleated on the surface of a ceramic boat placed in the temperature zone of 200 °C.

We next did scanning electron-microscope (SEM) measurements with a Hitachi S4800 Ultra-High Resolution Field Emission SEM. The crystallites have the highly-elongated, planar geometry and flat top surfaces typical of single crystals, as in Figure 1a. To test the crystals' stochiometry, we collected site-selected energy-dispersive X-ray (EDX) spectra. The Cd_3As_2 platelets are slightly Cd-enriched: the X-ray intensity ratio (Figure 1a) deviates slightly from the ideal 60:40 Cd-to-As atomic ratio seen in the polycrystalline Cd_3As_2 precursor.

We measured the platelets' optical absorption at room temperature in the spectral range of 100-500 meV, using the 2x transmission + reflection configuration discussed in Ref. [8] (measurement details appear in the supplementary material). The spectrum appears in Figure 1b. Above 350 meV, the absorption is primarily interband. At lower energy, the free-carrier absorption rises rapidly, reaching 30% (an absorption coefficient of 350 cm^{-1}) at 100 meV. Phonon absorption causes additional spectral features that look like noise in the low-energy range. The strong absorption observed throughout the mid-infrared means that sensors based on Cd_3As_2 will remain highly sensitive for long wavelengths, as they are for the 1064-nm light that we used to test them.

Having characterized our Cd_3As_2 crystals, we now turn to metal-semimetal-metal PTV devices, as shown in Figure 1c. A PTV sensor was made by placing a platelet of roughly 3 mm x 4 μm x 10 μm across the gap formed by two copper pads using micro-manipulators, and the platelet was permanently attached to the copper by melting indium at the contacts. The device schematic is presented in Figure 1c. We measured the dependence of the electrical conductivity, σ, on temperature, *T*, shown in Figure 2a. Our Cd_3As_2 behaves much like a metal: σ changed only slightly with T and $\frac{1}{\sigma}\frac{d\sigma}{dT}$ <0. Next, we measured a thermally induced Seebeck voltage to determine the temperature dependence of the thermopower (the magnitude |*S*| of the Seebeck coefficient) for temperatures of 300-500 K. The samples were placed in a cryostat at a base pressure of order 0.1 mTorr. We created a several-Kelvin difference across the sample by illuminating one of the metal electrodes with a continuous, 1064-nm laser. (This illumination is to the left of that illustrated in Figure 1c.) The measured thermopower appears in Figure 2a (inset), and exhibits a maximum at 385 K, which we attribute to ambipolar heat transport. As S<0,

a)

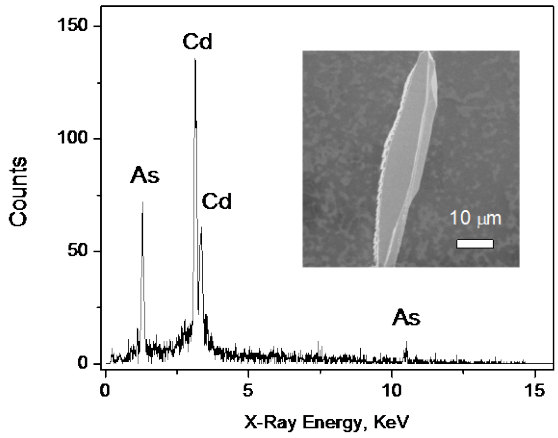

b)

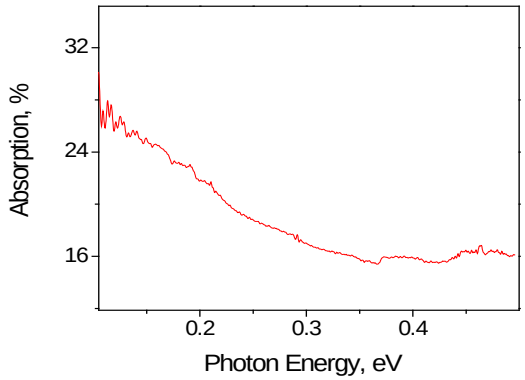

c)

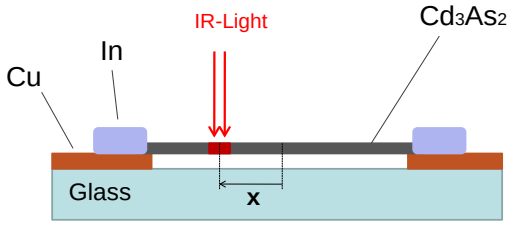

Figure 1. (a) EDX spectrum of a Cd_3As_2 platelet. The inset shows a top-view, high-resolution SEM image of the platelet; the bar is 10 μm. (b) Infared (FTIR) absorption spectrum of a Cd_3As_2 platelet. (c) A schematic of a Cd_3As_2 platelet sensor; X is the beam position measured from the device center.

electrons, the majority carriers, dominate the thermo-electric properties at low temperature. [6]

To characterize the operation of our devices as PTV sensors, current-voltage (I-V) data were collected using a Keithley 236 source-measure unit, with the applied bias usually not exceeding 10 mV to reduce Joule heating. Many platelets were tested, and the I-V characteristics remained non-rectifying, as shown in Figure 2b (and Figs. 1S and 3S, supplementary material). When the platelet is illuminated asymmetrically as illustrated in Figure 1c, an open-circuit voltage ΔV_{emf} of order 0.1 mV is readily registered; this confirms that the device operates as a solar cell. The net direct current, I_{dc}, generated by the sensor is given by:

$$I_{dc} = \frac{V_{bias} + \Delta V_{emf}}{R_{sensor} + R_c}, \qquad (1)$$

where V_{bias}, R_{sensor} and R_c stand for the applied bias, the resistance of Cd_3As_2, and the net contact electrical resistance, respectively, with $R_{sensor} >> R_c$. In the dark, ΔV_{emf} becomes zero and the current changes linearly with V_{bias}. Upon illumination (Figures 2b and 2c), the I-V curves remain Ohmic but shift vertically depending on the laser beam's position, X, measured from the device center. The short-circuit photocurrent changes linearly with X and reverses sign at X=0, where ΔV_{emf} =0. Indeed, when beam is positioned at X=0 the right and left temperature gradients are equal, and the two induced photovoltages cancel each other, yielding zero net current. Since S depends strongly on T (Figure 2a, inset), while the conductivity changes only slightly with T, the peak photocurrent occurs at 385 K, nearly the same temperature as the peak thermopower. At the operation temperature of ~ 300 K, the external DC responsivity—the ratio of the photocurrent to the incident optical power—is 0.27 mA/W. This value is close to the 0.5 mA/W reported for a similarly configured, two-terminal graphene sensor. [10]

a)

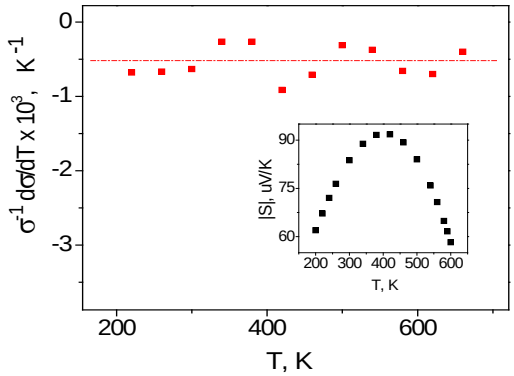

b)

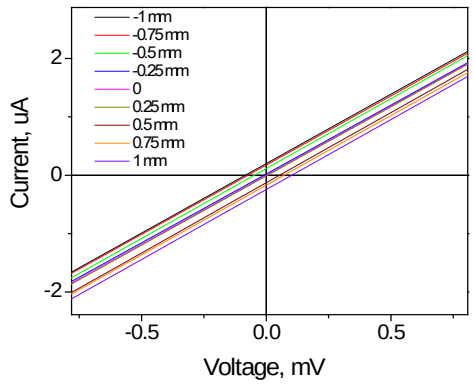

c)

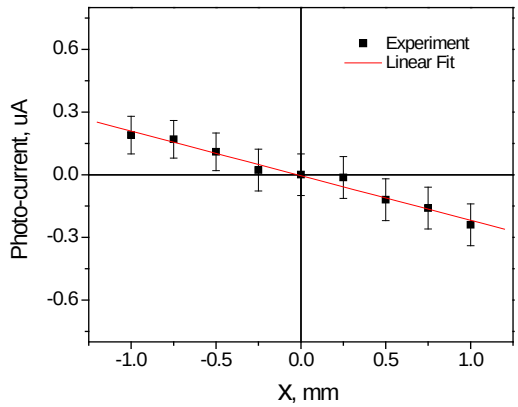

Figure 2. (a) $\frac{1}{\sigma}\frac{d\sigma}{dT}$ as a function of T, demonstrating metallic behavior. Inset: thermopower, |S|, as a function of T. (b) I-V characteristics obtained at different beam positions X. (c) Zero-bias photocurrent as a function of X; the red line is a linear fit to the data.

It should be mentioned that apart from the photo-induced Seebeck effect, other mechanisms to induce photocurrent include bolometric effects, electron-hole generation, and Schottky junctions. The bolometric effect arises from inelastic electron-phonon scattering processes that relax the free carriers' momentum, and should reduce the device's conductance with increasing light intensity. Indeed, we observe such a reduction (not shown), but it is very small, making the bolometric contribution to our photocurrent negligible. This reduction in conductance also rules out electron-hole generation as the cause of our photocurrent, as the generation of carriers would *increase* the conductivity, and would not vanish at X=0, as the measured photocurrent does. Likewise, we can exclude Schottky contacts as an origin of the photoresponse. In a Schottky diode, the I-V curves are highly non-linear, with both the forward and reverse saturation currents depending strongly on *T*. However, our I-V curves depend only weakly on temperature, and remain linear at bias up to 500 mV (Figs. S1-S3, supplementary material).

We assessed the PTV devices' room-temperature frequency response, which is of paramount importance for high-speed light switches and sensors, by performing on/off photocurrent measurements. According to Figure 3a, the ratio of transient (off-on-off) photocurrent, I_{photo} to root-mean-square dark current, *RMS*-I_{dark} is 25. At an incident power of 140 mW the room-temperature photocurrent was 38 uA (off/on measurements). Unlike PTV detectors based on carbon nanotubes or graphite studied previously [11,12], the photocurrent rises and falls sharply, with a response time much less than a second. To probe the high-frequency response, we modulated the incident intensity with an optical chopper and used lock-in detection. We used frequencies from 50 Hz to 6 kHz, applied no external bias, and measured the device's alternating short-circuit current, I_{SC}, as a function of frequency, f. Figure 3b shows the result: from 2 kHz to 6 kHz, $I_{SC} \sim f^{-\alpha}$, where α is 0.92±0.02, independent of the light intensity. We also

a)

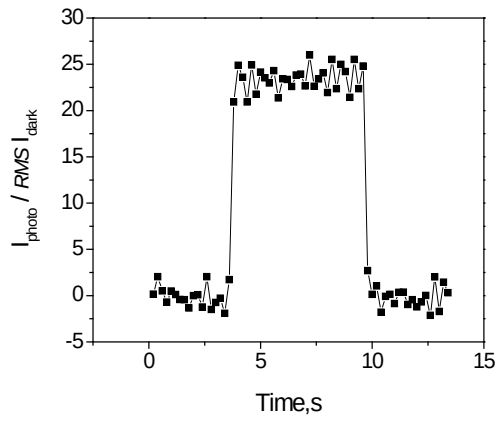

b)

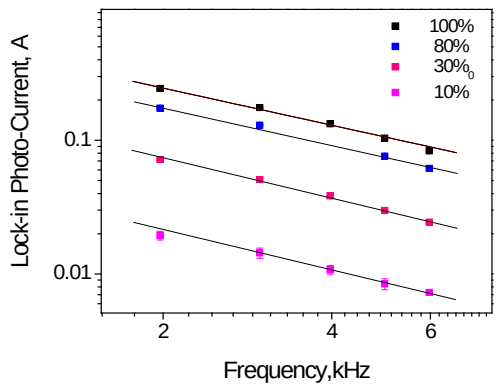

c)

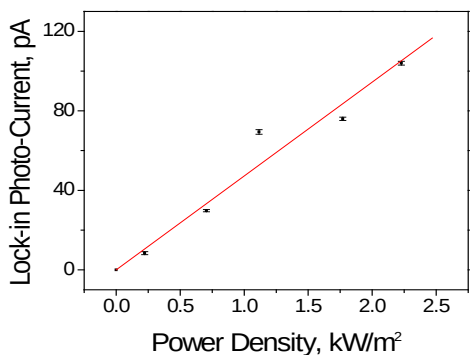

Figure 3. (a) The ratio of transient (off-on-off) photocurrent, I_{photo} to root-mean-square dark current, *RMS*-I_{dark}.(b) Lock-in photocurrent signal as a function of the modulation frequency for several excitation powers, log-log scale. The solid lines are best fits to $I_{SC} \sim f^{-\alpha}$, giving $\alpha = 0.92 \pm 0.02$. (c) Lock-in photocurrent vs. optical intensity. The light was chopped at a frequency of 4975 Hz; the red line is a linear fit to the data.

measured the photocurrent while varying P_{optical} with neutral density filters and modulating at high frequency. Figure 3c shows that, as expected, the photocurrent varies linearly with P_{optical}. As the sensor response time does not depend on P_{optical}, carrier-carrier scattering, such as Auger recombination, plays a negligible role. Though the photocurrent of the device decreases at high frequency, we show below that the intrinsic response time of Cd_3As_2 is fast, and that a much smaller PTV detector could approach terahertz bandwidth.

Note, first, that the bandwidth of a Cd_3As_2-based PTV sensor is not limited by its impedance, Z. Assuming negligible contact capacitance,

$$Z \cong R \,||\, C = \frac{R}{1+jRC\omega} \tag{2}$$

where $RC = \frac{\epsilon}{\sigma}$; $\varepsilon = 36\ \varepsilon_0$ and $\sigma = 2\text{x}10^5$ Sm are, respectively, the dielectric constant and room-temperature conductivity of Cd_3As_2. The circuit response time of the detector, τ_{RC}, is thus of order 10^{-15} s. For frequencies well below 10^{15} Hz (including all frequencies measured here), $Z \approx R$, so the detector's bandwidth is instead limited by the thermal response time of the Cd_3As_2 platelet, which determines the response time of ΔV_{emf}. In particular, in absence of carrier depletion regions, the detector's rise time is limited by both the RC-time, τ_{RC} and hot carrier transit/diffusion time, τ_{tr}: $\tau_r = \sqrt{\tau_{RC}^2 + \tau_{tr}^2}$. Here τ_{tr} is the time required to form temperature gradients across the device's channel. The upper bound of the device's frequency response is then $f_{\text{resp}} \cong 0.35/\tau_r$.

The shortest τ_r, and the fastest sensor, will be obtained for a channel whose length L is comparable to the diffusion length of photo-excited electrons, $d = \sqrt{D\tau_{el}}$, where D is the electronic diffusion coefficient and τ_{el} is the time in which a photoexcited electron exchanges energy with the crystal lattice. If the channel is much longer than the diffusion length, the temperature gradients take longer to form, while if the channel is

much shorter, thermal transport by photoexcited electrons will increase the thermal conductivity and degrade the sensitivity. If $L=d$, then $\tau_r = \frac{L^2}{D} = \frac{d^2}{D} = \tau_{el}$. We can estimate both the speed and the size of such a device based on ultrafast measurements that some of us reported in Ref. [9]. In that work hot electrons and holes were photoexcited by photons of energy 1.5 eV. After an initial relaxation of 0.5 ps, the electrons lost most of their energy to phonons in τ_{el} = 3.1 ps. Moreover, the diffusion coefficient was bounded as $D \leq 60$ cm^2/s. From this we conclude that a Cd_3As_2 –based PTV sensor optimized for speed should have a channel length $L \leq 130$ nm, and could operate at a frequency up to $f_{resp} \approx 0.1$ THz. This result indicates the possibility of dramatically increasing the detector's bandwidth.

Further improvements in the responsivity and wavelength selectivity of the PTV detectors may be afforded by pattering a detector's surface with plasmonic nanostructures. Such structures are known to induce strongly localized (spatially non-uniform) light heating, pushing the spatial resolution far below the light's wavelength and the response frequency into the terahertz range. [12,13]

In conclusion, we engineered a room-temperature infrared photosensor in Cd_3As_2 based on the photo-induced Seebeck effect. Its photo-response was successfully tested at the light modulations up to 6 kHz. The demonstrated detector is robust, requires no bias, and its responsivity to light reaches 0.27 mA/W. Cd_3As_2, because of its ultrafast response, is a promising material in which to further optimize such detectors' speed through miniaturization.

Acknowledgement: This work was supported by NSF ECCS and DMR Grants# 0621919 and 1508278, respectively.

References.

[1] G. B. Halász, L. Balents, Phys. Rev. B 85, 035103 (2012).

[2] Y. Sakamoto, T. Hirahara, H. Miyazaki, S. Kimura, S. Hasegawa, Phys. Rev. B 81, 165432 (2010).

[3] J. Wang, A. M. DaSilva, C. Chang, K. He, J. K. Jain, N. Samarth, X. Ma, Q. Xue, M. H. W. Chan Phys. Rev. B 83, 245438 (2011).

[4] T. Liang, Q. Gibson, M. Ali, M. Liu, R. Cava and N. Ong, Nature Materials, 14, 280 (2015).

[5] D. G. Schlom, L. N. Pfeiffer, Nature Mater. 9, 881 (2010).

[6] T. Hosseini, N. Yavarishad, J. Alward, N. Kouklin, Adv. Elec. Mat., 2 (2016).

[7] arXiv:1602.08951

[8] N.Kouklin, M. Tzolov, D. Straus, J. M. Xu, Appl. Phys. Lett., 85, 4463 (2004).

[9] C. P. Weber, E. Arushanov, B. S. Berggren, T. Hosseini, N. Kouklin, A. Nateprov, Appl. Phys. Lett., 106, 231904 (2015).

[10] F. Xia, T. Mueller, Y. Lin, A. Valdes-Garcia, P. Avouris, Nature Nanotechnology 4, 839 - 843 (2009).

[11] M. Omari, N. Kouklin, Appl. Phys. Lett., 98, 243113, (2011).

[12] T. Hosseini, N.Kouklin, Appl. Phys. Lett. 105, 043104, (2014).

[13] E. Barnard,W. Cai, Y.Jun, J.White and M. Brongersma, Nat. Mat., 9. 193 (2010)